


Article

CO₂ Capture from High-Humidity Flue Gas Using a Stable Metal–Organic Framework

Qi Wang, Yang Chen *, Puxu Liu, Yi Wang, Jiangfeng Yang, Jinping Li and Libo Li *

Shanxi Key Laboratory of Gas Energy Efficient and Clean Utilization, College of Chemical Engineering and Technology, Taiyuan University of Technology, Taiyuan 030024, China

* Correspondence: chenyang@tyut.edu.cn (Y.C.); lilibo@tyut.edu.cn (L.L.)

Abstract: The flue gas from fossil fuel power plants is a long-term stable and concentrated emission source of CO₂, and it is imperative to reduce its emission. Adsorbents have played a pivotal role in reducing CO₂ emissions in recent years, but the presence of water vapor in flue gas poses a challenge to the stability of adsorbents. In this study, ZIF-94, one of the ZIF adsorbents, showed good CO₂ uptake (53.30 cm³/g), and the calculated CO₂/N₂ (15:85, *v/v*) selectivity was 54.12 at 298 K. Because of its excellent structural and performance stability under humid conditions, the CO₂/N₂ mixture was still well-separated on ZIF-94 with a separation time of 30.4 min when the relative humidity was as high as 99.2%, which was similar to the separation time of the dry gas experiments (33.2 min). These results pointed to the enormous potential applications of ZIF-94 for CO₂/N₂ separation under high humidity conditions in industrial settings.

Keywords: CO₂ capture; ZIF; high humidity; stable structure



Citation: Wang, Q.; Chen, Y.; Liu, P.; Wang, Y.; Yang, J.; Li, J.; Li, L. CO₂ Capture from High-Humidity Flue Gas Using a Stable Metal–Organic Framework. *Molecules* **2022**, *27*, 5608. <https://doi.org/10.3390/molecules27175608>

Academic Editor: Wei-Yin Sun

Received: 3 August 2022

Accepted: 27 August 2022

Published: 31 August 2022

Publisher's Note: MDPI stays neutral with regard to jurisdictional claims in published maps and institutional affiliations.



Copyright: © 2022 by the authors. Licensee MDPI, Basel, Switzerland. This article is an open access article distributed under the terms and conditions of the Creative Commons Attribution (CC BY) license (<https://creativecommons.org/licenses/by/4.0/>).

1. Introduction

With the rapid growth of economic development needs and the world population, the world's energy demand is growing by leaps and bounds. Fossil energy will still account for more than 75% of total global energy consumption by 2040 [1]. The massive consumption of fossil energy leads to a continuous increase in the concentration of CO₂ and other greenhouse gases in the atmosphere, and its excessive emission contributes to the continuous increase in the greenhouse effect [2], which has negative impacts on the global climate. Because CO₂ is the most important of the greenhouse gases, reducing its emissions is regarded as the most important way to solve the climate problem. Therefore, doing so will also be an unavoidable responsibility and obligation in the next few years.

Among the various sources of CO₂, emissions of CO₂ in flue gas from coal-fired power plants account for 30–40% of the total [3]. The main components of flue gas tend to be around 12–15% CO₂, 85% N₂, and water vapor [4]. It is most effective and crucial to capture CO₂ from flue gas for storage due to its large and relatively concentrated CO₂ emissions. Carbon capture and storage (CCS) is one of the channels to achieving a reduction in CO₂ emissions. The key factor for significant progress lies in the choice of materials used to perform the separation. In this regard, the main methods for CO₂ separation are cryogenic fractionation [5], solvent absorption [6], sorbent adsorption [7], bioimmobilization [8], membrane permeation separation [9], and so on. The method of sorbent adsorption has received extensive attention due to its advantages of simple equipment, convenient operation, low energy consumption, and low corrosion and pollution. Zeolite, silica, BPL carbon, and metal–organic framework (MOF) are the most widely used adsorbents by far. In particular, zeolitic imidazolate frameworks [10,11] (ZIF as a subfamily of MOF) have many attractive properties such as high specific surface area, good structural stability, and flexibility that can be modified with functional groups by postsynthetic methods [12–15]. The framework structure can be rationally designed to achieve a large

range of pore sizes and three-dimensional (3-D) pore structures [16,17]. These are also the reasons why ZIF materials can be widely used for sensors [18,19], catalysts [20,21], catalyst supports, selective layers on catalysts via encapsulation [22,23], adsorbents [24–26], matrix fillers [27–29], membranes [30–37], and drug delivery systems [38–40]. ZIF materials play a pivotal role in the adsorption and separation of CO₂ under dry conditions based on these merits, such as ZIF-68–82 with the gmelinite (zeolite code GME) topology reported by Yaghi et al. [41]. The CO₂ adsorption capacity of ZIF-78 reached 49.03 cm³/g at 760 Torr and 298 K; they also reported two kinds of porous materials [42], ZIF-95 and ZIF-100, for which the adsorption capacities for CO₂ were 19.26 cm³/g and 21.28 cm³/g, respectively, under the conditions of 298 K and 1 bar.

Although many materials have impressive CO₂ capture capabilities in dry environments, it is worth mentioning that the presence of water in flue gas during practical applications, in addition to higher CO₂ capture capacity, makes it necessary to find novel adsorbents that have higher tolerance for humid environments. A few studies have been conducted on the hydrolytic stability of MOFs in humid environments. MIL-110/-101, CPO-27, and ZIF-8 are stable materials when exposed to water vapor for 2 h [43]. UiO-66-NH₂ [44] can maintain its original crystallinity and porous structure before and after water adsorption (relative humidity of 80%). MIL-100 [45] is completely water-stable owing to its trinuclear chromium clusters. The surface of MIL-53 is transformed, yielding H₂BDC and γ -AlO(OH) in boiling water [46]. ZIF-8 and ZIF-94 (also known as SIM-1) are stable after treatment in boiling water for at least 24 h [47–49]. Among them, the CO₂ adsorption capacity under dry conditions of ZIF-8 is 15.64 cm³/g at 298 K and 1 bar [50]; ZIF-94 also has the same SOD topology as ZIF-8. The former has a smaller pore size of the sodalite cavity due to the existence of the aldehyde group in the ligand, which may have a stronger force on CO₂ and further increase its CO₂ adsorption. However, there have been few reports on ZIF materials for CO₂/N₂ separation in humid environments.

Therefore, ZIF-94 was synthesized at room temperature using methanol and tetrahydrofuran as solvents in this paper. First, its stability was explored in humid and harsh chemical environments; the gas adsorption performance was then studied, and finally, the adsorption/separation performance of the material for CO₂/N₂ mixtures in dry and high humidity environments was studied in detail, confirming that the presence of water vapor has negligible influence on the CO₂ enrichment process. The above conclusions confirmed that ZIF-94 was a promising candidate for capturing CO₂ from high-humidity flue gas by virtue of its satisfactory structural stability and reusability.

2. Results and Discussion

2.1. Synthesis, Structure, and Characterization

ZIF-94 consisted of Zn tetrahedra linked by carboxylimidazolates forming a 3-D zeolitic imidazolate framework crystallizing in a sodalite topology [51,52]—see Figure 1a. ZIF-94 was built by combining experimental and computational methods, and it is isostructural to ZIF-8 (SOD), which is commercialized under the name Basolite Z-1200™ [12]. ZIF-8 has a methyl group at position 2, whereas ZIF-94 contains a methyl and an aldehyde in positions 4 and 5, respectively. The simulation indicated a pore size of the sodalite cavity of 8.0 Å for ZIF-94 against 11.3 Å for ZIF-8, and the difference in the imidazole group resulted in a smaller cavity for the former [53,54]. As shown in Figure S1, the ZIF-94 was synthesized at room temperature using methanol and tetrahydrofuran, and 3.67 g of product could be synthesized at one time; it has the potential for large-scale synthesis. The freshly synthesized sample appeared as a white crystalline powder, and its powder X-ray diffraction (PXRD) is shown in Figure 1b. The diffraction peaks of the synthesized and activated samples were consistent with the simulation peak of ZIF-94, and the peak shape was relatively sharp, indicating that the sample under this condition had high crystallinity and purity. Scanning electron microscopy (SEM) revealed the morphology and size of ZIF-94. Figure S2 shows that the ZIF-94 crystal had a 3-D structure of a dodecahedron with a smooth surface and a particle size of about 4 nm. The N₂ adsorption isotherm at 77 K

showed the microporous structure of the material (Figure 1c) with a BET surface area of $588 \text{ m}^2/\text{g}$, which was comparable to the reported value [55]. The thermogravimetric (TG) curve of the material in Figure 1d showed the two weight loss steps in the decomposition process. The first may be attributed to the loss of the solvents CH_3OH and H_2O in the pores of ZIF-94, and the second may be due to the disintegration of the structure. However, the sample was thermally stable below $400 \text{ }^\circ\text{C}$. ZIF-94 synthesized at room temperature with a stable structure offers the possibility for the adsorption and separation of CO_2 under actual industrial conditions.

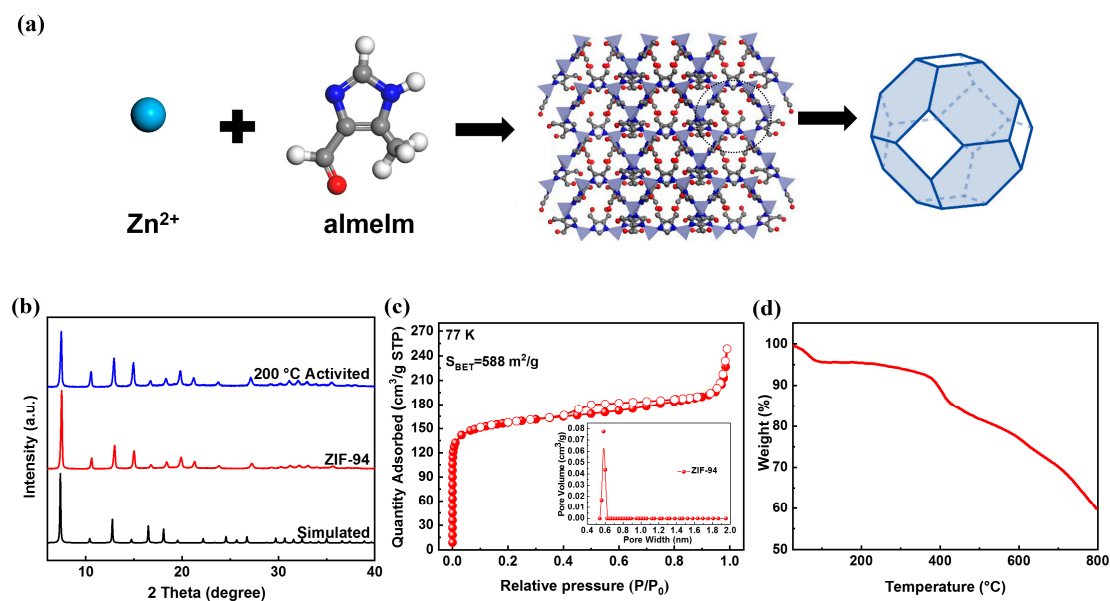


Figure 1. (a) The structure of ZIF-94. (b) The PXRD of freshly synthesized samples and activated samples. (c) The N_2 adsorption isotherm of ZIF-94 at 77 K . (d) TGA data obtained for ZIF-94.

2.2. Gas Adsorption Performance

Based on the pore structure and configuration of ZIF-94, the adsorption isotherms of CO_2/N_2 were studied at different temperatures (273 and 298 K) and 1 bar . Figure 2a shows the adsorption isotherms of CO_2 and N_2 at 298 K and 1 bar . ZIF-94 showed high CO_2 uptake ($53.30 \text{ cm}^3/\text{g}$) and low N_2 uptake ($6.39 \text{ cm}^3/\text{g}$), giving an excellent uptake ratio of CO_2 over N_2 (8.34), indicating that the structure had a unique adsorption affinity for CO_2 . An adsorption test was performed at 273 K under the same conditions to study the adsorption performance of the material further, as presented in Figure 2b. Notably, lower temperatures led to higher adsorption capacity for the same component, and for N_2 under the same conditions, the adsorption capacity of CO_2 was still higher than that of the former. In addition, the adsorption and desorption isotherms of CO_2 and N_2 at the two temperatures overlapped completely, and it could be clearly seen that the adsorption–desorption process of the material could be accomplished perfectly, which could reduce energy consumption and provide the possibility of implementing the adsorption–desorption cycle of the adsorbent in industry. Subsequently, ideal adsorbed solution theory (IAST) calculations were performed using the fitted parameters of the two-site Langmuir–Freundlich isotherm model (Tables S1 and S2) to predict the selectivity of the CO_2/N_2 mixture at different temperatures (273 and 298 K) and 1 bar . As shown in Figure 2c, the calculated CO_2/N_2 ($15:85$, v/v) selectivities were 67.11 and 54.12 at 273 and 298 K , and the calculated CO_2/N_2 ($50:50$, v/v) selectivities were 87.44 and 95.29 at 273 and 298 K , respectively. The Langmuir–Freundlich parameters are shown in Figure S3 and gave satisfactory agreement ($R^2 > 0.999$). Therefore, the CO_2 -selective adsorbents were compared in terms of CO_2 adsorption capacity and selectivity, as shown in Table S3, outperforming previously reported benchmark materials with GME topology (such as ZIF-78 and ZIF-82), which showed the great potential of ZIF-94 in CO_2/N_2 separation. In addition, the

heats of adsorption of CO₂ and N₂ of ZIF-94 as shown in Figure 2d were calculated using the Clausius–Clapeyron equation. In the near-zero adsorption region, the adsorption heats of ZIF-94 for CO₂ and N₂ were 28.23 kJ/mol and 15.71 kJ/mol, respectively. On the one hand, this showed that ZIF-94 was a CO₂-selective adsorbent, and on the other hand, the relatively low adsorption heat was beneficial to the desorption regeneration of the adsorbent during the separation process, and the view was also confirmed that the above adsorption–desorption isotherms were completely coincident (Figure 2a,b), further reducing the energy consumption. In addition, ZIF-94 showed high adsorption capacity and high IAST selectivity for CO₂/N₂ mixtures, making it an excellent potential adsorbent for high-humidity applications.

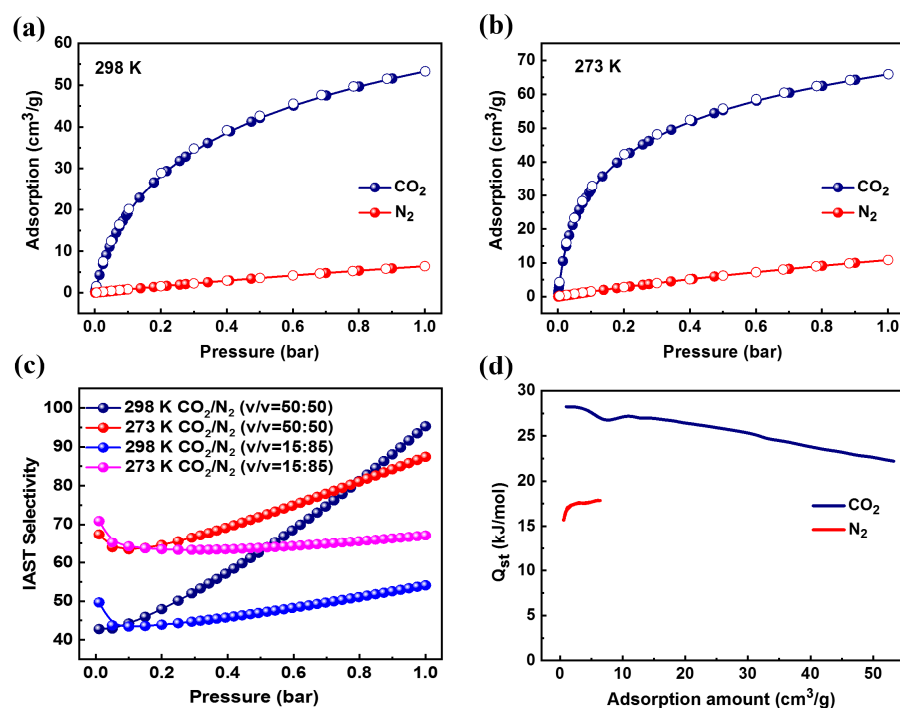


Figure 2. (a) The adsorption isotherms of CO₂ and N₂ at 298 K and 1 bar. (b) The adsorption isotherms of CO₂ and N₂ at 273 K and 1 bar. (c) The calculated CO₂/N₂ selectivity at 273 and 298 K. (d) The isosteric heats of adsorption (Q_{st}) for ZIF-94.

2.3. Dynamic Breakthrough Experiments for CO₂/N₂ Mixtures

The previous experiments demonstrated that ZIF-94 has high CO₂ adsorption capacity and satisfactory CO₂/N₂ selectivity; the phenomena prompted us to investigate the feasibility of using ZIF-94 in the separation process under humid conditions. Two types of wet breakthrough experiments for CO₂/N₂ (15/85; v/v) were conducted in this section (Figure S4), dry gas and wet gas (99.2%), to evaluate the gas-separation performance under ambient conditions. The feed gas of CO₂/N₂ was passed through the adsorption column loaded with activated ZIF powder at a total flow rate of 5 mL/min at 298 K and 1 bar. For the dry gas experiments, as shown in Figure 3a, N₂ was initially eluted through the adsorption column at 1.4 min and then reached saturation, whereas CO₂ was selectively adsorbed on the column at both compositions until 33.2 min. At the same time, the CO₂/N₂ mixture could be efficiently separated to obtain high-purity CO₂ within these time intervals. In addition, the gas adsorption capacity of CO₂ on ZIF-94 reached 32.76 cm³/g in dynamic breakthrough experiment. This indicated that during the dynamic adsorption process of the mixed gas, ZIF-94 displayed a stronger adsorption affinity for CO₂ than for N₂. Afterward, desorption experiments on CO₂/N₂ mixtures purging the column with Ar at a flow rate of 10 mL/min were conducted under ambient conditions. As shown in Figure 3c, the concentration of N₂ dropped sharply to achieve N₂ desorption in preference to CO₂

during the purging time of 9.7 min. Similarly, we could obtain purified CO₂ at the outlet of the adsorption column until purging for 34.0 min. ZIF-94 achieved desorption of CO₂ by room-temperature purging in a short time, which provides the possibility of its repeated use in industry.

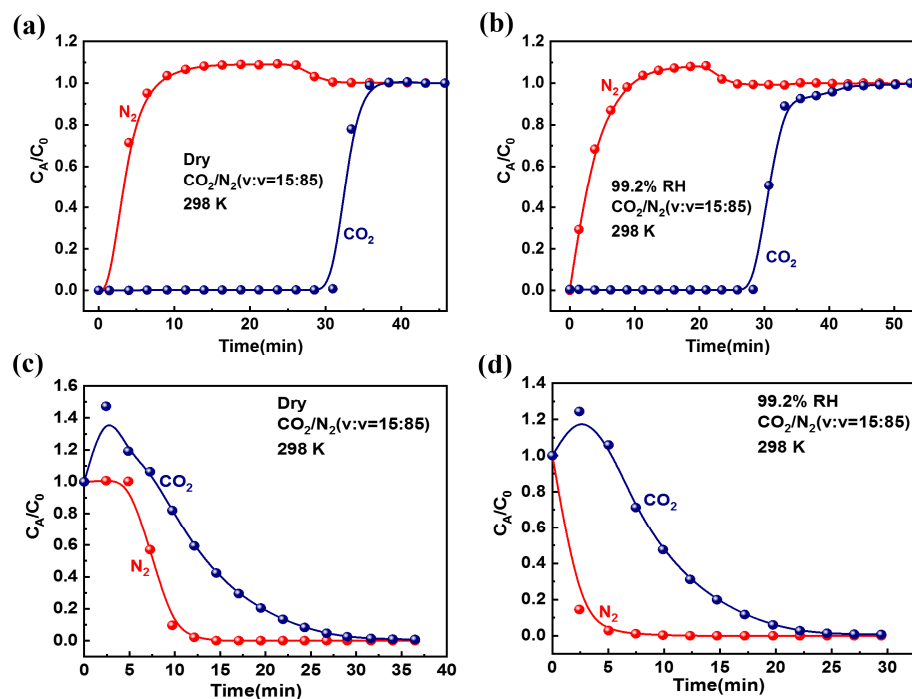


Figure 3. Experimental breakthrough and desorption curves for CO₂/N₂ mixture (15/85, v/v) under two humidity conditions: (a,c) dry gas and (b,d) wet gas (99.2% RH).

As a major source of CO₂, flue gas is particularly important with regard to CO₂ capture. However, the presence of water in flue gas imposes higher requirements for the CO₂ adsorbent; it is still necessary to maintain its CO₂ capture capacity under wet conditions. To make the ZIF-94 more suitable for practical application, a mixture of CO₂/N₂/H₂O(v) under aqueous conditions (RH = 99.2%) was studied, and the rest of the conditions were consistent with the above dry experiments. For the wet gas (99.2%) experiments, as shown in Figure 3b, N₂ and CO₂ were first detected through the adsorption column at 1.4 min and 30.4 min, respectively. The dynamic saturated adsorption amounts of CO₂ and N₂ are 30.94 and 5.74 cm³/g, respectively, and the dynamic selectivity is 30.54. We were delighted to discover that the CO₂/N₂ mixture was still well-separated on ZIF-94 when the relative humidity was 99.2%, and the separation time (30.4 min) was similar to the separation time of the dry gas experiments (33.2 min). A possible cause of this phenomenon was that the presence of -CH₃, a hydrophobic group, makes ZIF-94 insensitive to water molecules. At the same time, it showed its poor adsorption capacity for water vapor at room temperature and pressure (Figure S5). It is worth mentioning that the breakthrough curve in a humid environment showed a longer tail, revealing that the adsorption dynamics were also impacted by water, which was attributed to the increased dependence on molecular mass transfer caused by saturation of the outer adsorbent layer [56]. Figure 3d shows CO₂ at the outlet of the adsorption column until purging at 29.4 min in the desorption experiments, a slightly shorter time than in the dry gas experiments (Figure 3c). In summary, the two types of wet breakthrough experiments showed similar characteristics regardless of the humidity, and it was inferred that water vapor adsorption had no effect on the separation of CO₂/N₂; ZIF-94 had excellent water resistance while maintaining its gas separation performance capture capability in wet conditions.

2.4. Structural and Performance Stability Investigations

In addition to the potential for large-scale synthesis of ZIF-94 at room temperature, we also needed to evaluate it in terms of structural stability and performance stability, so that it can be better used in the separation of CO₂ in flue gas. In the structural stability assessment, as shown in Figure 4a, the PXRD pattern obtained after being exposed to air for half a year (Figure S6) was still in good agreement with the freshly synthesized sample and had no impurity peaks, indicating that the sample has excellent stability in air. Destruction of the sample structure is often caused by the presence of water molecules, so the stability test of ZIF-94 was conducted in a humid environment. The samples were immersed in water for 1 day, 3 days, 7 days, 1 month, and 2 months (Figure S7); the test results showed that the crystallinity of the sample basically did not change with the prolongation of soaking time. The PXRD patterns of the sample were analyzed after activation at different temperatures (Figure S8), and the PXRD patterns under these conditions are still consistent with the simulated peaks. Moreover, the chemical stability of ZIF-94 was evaluated by treating the samples under harsh conditions. Their PXRD patterns also remained intact after soaking in different pH solutions for 2 days (Figures S9 and S10), and there was no phase transition or structural collapse, demonstrating the material's resistance to harsh chemical environments. The PXRD patterns of the samples after multiple adsorptions and dynamic breakthrough experiments were compared with those of the freshly synthesized samples, and the intensity of the diffraction peaks was still well-maintained, it can be seen that the above two processes could not destroy the crystal structure. In short, ZIF-94 exhibited satisfactory structural stability, excellent thermal stability, and exceptional recoverability in water and aqueous alkaline solutions. At the same time, ZIF-94 also preliminarily showed that it was a promising candidate for adsorption and separation under high humidity conditions by virtue of its water resistance.

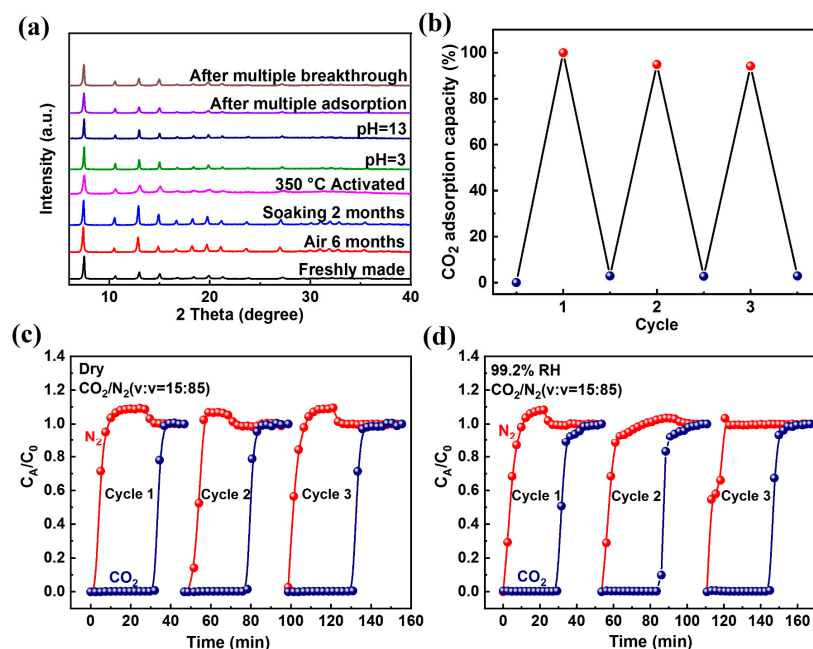


Figure 4. (a) Corresponding PXRD patterns to show the maintained structure of ZIF-94 under different conditions. (b) Cycling adsorption isotherms for CO₂ at 298 K and 1 bar. Cycling breakthrough experiments on CO₂/N₂ mixture (15/85, *v/v*) under two humidity conditions: (c) dry gas and (d) wet gas (99.2% RH).

In the performance stability assessment, first, we performed single-component adsorption cycle experiments of CO₂ at 298 K and 1 bar. As shown in Figure 4b, the adsorption capacity of CO₂ hardly decreased in adsorption cycling experiments, indicating its good structural stability and reusability. Furthermore, component adsorption of CO₂ was per-

formed on ZIF-94 under different conditions, as shown in Figure S11. It was found that the CO₂ adsorption amount of the sample exposed to the air for 4 months was 49.59 cm³/g, and the sample soaked in water for 2 months at room temperature (56.33 cm³/g) was close to that of the freshly made sample (53.30 cm³/g), which further confirms that ZIF-94 maintains its original adsorption capacity in a high-humidity environment. Finally, Figure 4c,d displays cyclic breakthrough experiments using a CO₂/N₂ mixture (15/85, v/v) under the two humidity conditions three times, and the breakthrough time was almost constant, which confirms that the presence of water vapor has negligible influence on the CO₂ enrichment process. The performed N₂ adsorption–desorption experiments proved that the N₂ adsorption amount of the material remained unchanged (Figure S12), and it maintained its initial porous structure. Moreover, ZIF-94 could repeatedly achieve separation of CO₂/N₂ without loss of performance in both dry and humid environments. The above test results indicated the excellent cycle performance of ZIF-94, coupled with its robust structural stability. The excellent cycle performance for CO₂ adsorption and separation points to the enormous potential applications of ZIF-94 for CO₂/N₂ separation under humid conditions in industrial settings.

3. Materials and Methods

3.1. Preparation of ZIF-94

The synthetic methods described in the literature [55,57–60] were modified as follows: ZIF-94: 2.64 g of Zn(CH₃COO)₂·2H₂O (12 mmol) was dissolved in 20 mL methanol, and 2.64 g of 4-methyl-5-imidazolecarboxaldehyde (48 mmol) was dissolved in 50 mL tetrahydrofuran. The methanol solution was added to the tetrahydrofuran solution under vigorous stirring. Afterward, the mixture was continuously stirred at room temperature for 16 h. The pale yellow precipitate was filtered and washed with methanol three times. The resulting sample was dried at room temperature in air for 48 h.

3.2. Characterization

The crystal structure and crystallinity of the sample were measured using PXRD on a Bruker D8 ADVANCE X-ray diffractometer with a Cu K α radiation source ($\lambda = 1.5418 \text{ \AA}$). Scanning was performed over a 2θ range of 5–40° at a scanning rate of 4°/min. Thermogravimetric analysis (TGA) of the sample was carried out on a thermal analyzer (NETZSCH STA 449F5). The sample was heated at a rate of 10 °C/min in an N₂ atmosphere. The morphology of the as-synthesized sample was observed and confirmed using SEM on a Hitachi SU8010 instrument. N₂ adsorption–desorption isotherms were recorded at 77 K on Micromeritics ASAP 2460 and 3020 instruments. Water-adsorption isotherms at 298 K were measured using an automated volumetric adsorption apparatus (Quantachrome). Before measurement, the sample was degassed at 200 °C for 12 h until the residual pressure was below 1×10^{-6} Torr and all gases were of 99.999% purity.

3.3. Adsorption and Breakthrough Experiments

Single-component gas adsorption isotherms for CO₂ and N₂ were recorded on a Micromeritics ASAP 2020 instrument at 273 K and 298 K. The sample was activated at 200 °C under a high vacuum (10^{-6} Torr) for 12 h until no weight loss was observed. High purity CO₂ (99.999%) and N₂ (99.999%) were used in the gas adsorption experiments. Before the breakthrough experiments, the sample was degassed and activated at 200 °C for 12 h, and then cooled to room temperature. Approximately 0.7147 g of each sample was loaded into a stainless-steel adsorption column with an inner diameter of 4.57 mm and a length of 120 mm. High purity Ar was used to purge the column at a flow rate of 10 mL/min to remove any residual gas in the pipeline. The adsorption columns loaded with each sample were fixed in an in-house-built device. The flow rate of CO₂ and N₂ was adjusted using a pressure valve and flowmeter located at the inlet of the adsorption column. The concentration of CO₂ and N₂ was monitored in real time using gas chromatography (490 Micro GC, Palo Alto, CA, USA) at the outlet of the adsorption column. Each experiment

was carried out at 298 K, and the flow rate of the CO₂/N₂ mixture (15:85, *v/v*) was 5 mL/min until saturation was reached (Figure S4). Subsequently, the adsorption bed was regenerated using Ar (10 mL/min). In addition, after the adsorption and breakthrough experiments, the sample was removed, weighed, and analyzed using PXRD.

3.4. Ideal Adsorbed Solution Theory Calculations

The single-component adsorption isotherms of CO₂ and N₂ on ZIF-94 obtained at 273 K and 298 K were fitted using the dual site Langmuir–Freundlich model proposed by Myers [61] et al.:

$$q = q_{A,sat} \frac{b_A p^{\nu A}}{1 + b_A p^{\nu A}} + q_{B,sat} \frac{b_B p^{\nu B}}{1 + b_B p^{\nu B}}$$

where q represents the adsorbed capacity per mass of adsorbent (mol/kg), $q_{A,sat}$ and $q_{B,sat}$ are the saturation uptake capacities at sites A and B, respectively, b_A and b_B represent the constant at adsorption sites A and B, respectively (Figure S3), P represents the total pressure of the gas at equilibrium (kPa), and ν represents the Freundlich exponent.

The adsorption selectivity is defined as follows:

$$S_{ads} = \frac{q_A/q_B}{y_A/y_B}$$

where q_A and q_B represent the component molar loadings within the MOF, and y_A and y_B are the corresponding mole fractions used in the feed gas mixture.

The parameters are provided in Tables S1 and S2.

4. Conclusions

In this work, ZIF-94 was synthesized at room temperature using methanol and tetrahydrofuran as solvents. ZIF-94 exhibited satisfactory structural stability, excellent thermal stability, and exceptional recoverability in water and aqueous alkaline solutions. The CO₂ uptake and low N₂ uptake at 298 K and 1 bar were 53.30 cm³/g and 6.39 cm³/g, respectively. The calculated CO₂/N₂ (15:85, *v/v*) selectivities were 67.11 and 54.12 at 273 and 298 K, respectively. The separation time (30.4 min) for the wet gas (99.2%) experiments was similar to the separation time for the dry gas experiments (33.2 min) in dynamic breakthrough experiments for CO₂/N₂ mixtures. The CO₂ adsorption amount of the sample soaked in water for 2 months at room temperature (56.33 cm³/g) was close to that of the freshly made sample (53.30 cm³/g). The presence of water molecules did not affect the adsorption and separation processes of CO₂ on ZIF-94. ZIF-94 has been shown to be a kind of adsorbent that has the requisite hydrolytic stability for applications in high-humidity environments.

Supplementary Materials: The following supporting information can be downloaded at: <https://www.mdpi.com/article/10.3390/molecules27175608/s1>, Figure S1: Schematic representation of synthesis of ZIF-94 at room temperature; Figure S2: SEM of as-synthesized ZIF-94; Figure S3: CO₂ (a, 298 K, and b, 273 K) and N₂ (c, 298 K, and d, 273 K) adsorption isotherms in ZIF-94 with dual-site Langmuir–Freundlich model fits; Figure S4: Diagram of breakthrough experimental apparatus; Figure S5: H₂O adsorption of ZIF-94 at 298 K; Figure S6: PXRD of ZIF-94 exposed to air for 4 months and 6 months; Figure S7: PXRD of ZIF-94 soaked in water for 1, 3, 7, 30, and 60 days; Figure S8: PXRD of ZIF-94 activated at different temperatures; Figure S9: Images of ZIF-94 before and after soaking in different pH solutions. (a) before soaking, (b) after soaking for 2 days; Figure S10: PXRD of ZIF-94 soaked in solutions with different PH values; Figure S11: The adsorption isotherms of CO₂ under different conditions; Figure S12: The N₂ adsorption isotherm at 77 K of the samples. (a) Freshly made, (b) Multiple adsorption experiments, (c) Dynamic breakthrough experiments; Table S1: Dual-Langmuir–Freundlich fitting parameters for CO₂ and N₂ in ZIF-94 at 298 K; Table S2: Dual-Langmuir–Freundlich fitting parameters for CO₂ and N₂ in ZIF-94 at 273 K; Table S3: Comparison of CO₂ adsorption uptakes and selectivity for CO₂/N₂ around the top-performing ZIF; Table S4: Some typical materials with high CO₂ adsorption capacity. References [13,62–80] are cited in supplementary materials.

Author Contributions: Conceptualization, Q.W. and L.L.; formal analysis, J.Y. and Y.W.; investigation, Q.W. and P.L.; resources, J.L. and L.L.; data curation, Y.C. and P.L.; writing—original draft preparation, Q.W.; writing—review and editing, L.L., Y.C. and Q.W.; supervision, J.L. All authors have read and agreed to the published version of the manuscript.

Funding: This research was funded by National Natural Science Foundation of China (grant numbers 22090062, 21922810, 21908155); Research project supported by the Shanxi Scholarship Council of China (grant number 2021-053).

Institutional Review Board Statement: Not applicable.

Informed Consent Statement: Not applicable.

Data Availability Statement: The data presented in this study are available on request from the corresponding author.

Conflicts of Interest: The authors declare no conflict of interest.

Sample Availability: Samples of the compounds are not available from the authors.

References

1. Abas, N.; Kalair, A.; Khan, N. Review of fossil fuels and future energy technologies. *Futures* **2015**, *69*, 31–49. [[CrossRef](#)]
2. Sircar, S. Basic research needs for design of adsorptive gas separation processes. *Ind. Eng. Chem. Res.* **2006**, *45*, 5435–5448. [[CrossRef](#)]
3. Aaron, D.; Tsouris, C. Separation of CO₂ from flue gas: A review. *Sep. Sci. Technol.* **2005**, *40*, 321–348. [[CrossRef](#)]
4. Nguyen, T.T.; Lin, J.-B.; Shimizu, G.K.; Rajendran, A. Separation of CO₂ and N₂ on a hydrophobic metal organic framework CALF-20. *Chem. Eng. J.* **2022**, *442*, 136263. [[CrossRef](#)]
5. Song, C.; Kitamura, Y.; Li, S. Energy analysis of the cryogenic CO₂ capture process based on Stirling coolers. *Energy* **2014**, *65*, 580–589. [[CrossRef](#)]
6. Linneen, N.; Pfeffer, R.; Lin, Y. CO₂ capture using particulate silica aerogel immobilized with tetraethylenepentamine. *Microporous Mesoporous Mater.* **2013**, *176*, 123–131. [[CrossRef](#)]
7. Nittaya, T.; Douglas, P.L.; Croiset, E.; Ricardez-Sandoval, L.A. Dynamic modelling and control of MEA absorption processes for CO₂ capture from power plants. *Fuel* **2014**, *116*, 672–691. [[CrossRef](#)]
8. Benemann, J.R. Utilization of carbon dioxide from fossil fuel-burning power plants with biological systems. *Energy Convers. Manag.* **1993**, *34*, 999–1004. [[CrossRef](#)]
9. Ahmad, A.; Jawad, Z.; Low, S.; Zein, S. A cellulose acetate/multi-walled carbon nanotube mixed matrix membrane for CO₂/N₂ separation. *J. Membr. Sci.* **2014**, *451*, 55–66. [[CrossRef](#)]
10. Davis, M.E. Ordered porous materials for emerging applications. *Nature* **2002**, *417*, 813–821. [[CrossRef](#)]
11. Grubert, G.; Stockenhuber, M.; Tkachenko, O.P.; Wark, M. Titanium oxide species in molecular sieves: Materials for the optical sensing of reductive gas atmospheres. *Chem. Mater.* **2002**, *14*, 2458–2466. [[CrossRef](#)]
12. Huang, X.C.; Lin, Y.Y.; Zhang, J.P.; Chen, X.M. Ligand-directed strategy for zeolite-type metal–organic frameworks: Zinc (II) imidazolates with unusual zeolitic topologies. *Angew. Chem. Int. Ed.* **2006**, *45*, 1557–1559. [[CrossRef](#)] [[PubMed](#)]
13. Banerjee, R.; Phan, A.; Wang, B.; Knobler, C.; Furukawa, H.; O’Keeffe, M.; Yaghi, O.M. High-throughput synthesis of zeolitic imidazolate frameworks and application to CO₂ capture. *Science* **2008**, *319*, 939–943. [[CrossRef](#)]
14. Peralta, D.; Chaplais, G.; Simon-Masseron, A.; Barthelet, K.; Chizallet, C.; Quoineaud, A.-A.; Pirngruber, G.D. Comparison of the behavior of metal–organic frameworks and zeolites for hydrocarbon separations. *J. Am. Chem. Soc.* **2012**, *134*, 8115–8126. [[CrossRef](#)] [[PubMed](#)]
15. Rowsell, J.L.; Yaghi, O.M. Effects of functionalization, catenation, and variation of the metal oxide and organic linking units on the low-pressure hydrogen adsorption properties of metal–organic frameworks. *J. Am. Chem. Soc.* **2006**, *128*, 1304–1315. [[CrossRef](#)]
16. Liu, Y.; Kravtsov, V.C.; Larsen, R.; Eddaoudi, M. Molecular building blocks approach to the assembly of zeolite-like metal–organic frameworks (ZMOFs) with extra-large cavities. *Chem. Commun.* **2006**, *14*, 1488–1490. [[CrossRef](#)]
17. Tian, Y.Q.; Zhao, Y.M.; Chen, Z.X.; Zhang, G.N.; Weng, L.H.; Zhao, D.Y. Design and generation of extended zeolitic metal–organic frameworks (ZMOFs): Synthesis and crystal structures of zinc (II) imidazolate polymers with zeolitic topologies. *Chem. A Eur. J.* **2007**, *13*, 4146–4154. [[CrossRef](#)]
18. Hwang, Y.; Sohn, H.; Phan, A.; Yaghi, O.M.; Candler, R.N. Dielectrophoresis-assembled zeolitic imidazolate framework nanoparticle-coupled resonators for highly sensitive and selective gas detection. *Nano Lett.* **2013**, *13*, 5271–5276. [[CrossRef](#)]
19. Fu, Y.; Dai, J.; Ge, Y.; Zhang, Y.; Ke, H.; Zhang, W. A novel non-enzymatic electrochemical hydrogen peroxide sensor based on a metal-organic framework/carbon nanofiber composite. *Molecules* **2018**, *23*, 2552. [[CrossRef](#)]
20. Karagiari, O.; Lalonde, M.B.; Bury, W.; Sarjeant, A.A.; Farha, O.K.; Hupp, J.T. Opening ZIF-8: A catalytically active zeolitic imidazolate framework of sodalite topology with unsubstituted linkers. *J. Am. Chem. Soc.* **2012**, *134*, 18790–18796. [[CrossRef](#)]
21. Silva, D.F.; Viana, A.M.; Santos-Vieira, I.; Balula, S.S.; Cunha-Silva, L. Ionic Liquid-Based Polyoxometalate Incorporated at ZIF-8: A Sustainable Catalyst to Combine Desulfurization and Denitrogenation Processes. *Molecules* **2022**, *27*, 1711. [[CrossRef](#)] [[PubMed](#)]

22. Kuo, C.-H.; Tang, Y.; Chou, L.-Y.; Sneed, B.T.; Brodsky, C.N.; Zhao, Z.; Tsung, C.-K. Yolk-shell nanocrystal@ ZIF-8 nanostructures for gas-phase heterogeneous catalysis with selectivity control. *J. Am. Chem. Soc.* **2012**, *134*, 14345–14348. [[CrossRef](#)] [[PubMed](#)]
23. Lu, G.; Li, S.; Guo, Z.; Farha, O.K.; Hauser, B.G.; Qi, X.; Wang, Y.; Wang, X.; Han, S.; Liu, X. Imparting functionality to a metal-organic framework material by controlled nanoparticle encapsulation. *Nat. Chem.* **2012**, *4*, 310–316. [[CrossRef](#)]
24. Gucuyener, C.; Van Den Bergh, J.; Gascon, J.; Kapteijn, F. Ethane/ethene separation turned on its head: Elective ethane adsorption on the metal-organic Framework ZIF-7 through a gate-opening mechanism. *J. Am. Chem. Soc.* **2010**, *132*, 17704–17706. [[CrossRef](#)]
25. Li, J.-R.; Ma, Y.; McCarthy, M.C.; Sculley, J.; Yu, J.; Jeong, H.-K.; Balbuena, P.B.; Zhou, H.-C. Carbon dioxide capture-related gas adsorption and separation in metal-organic frameworks. *Coord. Chem. Rev.* **2011**, *255*, 1791–1823. [[CrossRef](#)]
26. Wang, X.; Zhao, Y.; Sun, Y.; Liu, D. Highly Effective Removal of Ofloxacin from Water with Copper-Doped ZIF-8. *Molecules* **2022**, *27*, 4312. [[CrossRef](#)] [[PubMed](#)]
27. Li, T.; Pan, Y.; Peinemann, K.-V.; Lai, Z. Carbon dioxide selective mixed matrix composite membrane containing ZIF-7 nano-fillers. *J. Membr. Sci.* **2013**, *425*, 235–242. [[CrossRef](#)]
28. Kang, C.-H.; Lin, Y.-F.; Huang, Y.-S.; Tung, K.-L.; Chang, K.-S.; Chen, J.-T.; Hung, W.-S.; Lee, K.-R.; Lai, J.-Y. Synthesis of ZIF-7/chitosan mixed-matrix membranes with improved separation performance of water/ethanol mixtures. *J. Membr. Sci.* **2013**, *438*, 105–111. [[CrossRef](#)]
29. Zhang, L.; Hu, Z.; Jiang, J. Metal-organic framework/polymer mixed-matrix membranes for H₂/CO₂ separation: A fully atomistic simulation study. *J. Phys. Chem. C* **2012**, *116*, 19268–19277. [[CrossRef](#)]
30. Bux, H.; Feldhoff, A.; Cravillon, J.; Wiebcke, M.; Li, Y.-S.; Caro, J. Oriented zeolitic imidazolate framework-8 membrane with sharp H₂/C₃H₈ molecular sieve separation. *Chem. Mater.* **2011**, *23*, 2262–2269. [[CrossRef](#)]
31. Pan, Y.; Liu, Y.; Zeng, G.; Zhao, L.; Lai, Z. Rapid synthesis of zeolitic imidazolate framework-8 (ZIF-8) nanocrystals in an aqueous system. *Chem. Commun.* **2011**, *47*, 2071–2073. [[CrossRef](#)] [[PubMed](#)]
32. Kwon, H.T.; Jeong, H.-K. In situ synthesis of thin zeolitic-imidazolate framework ZIF-8 membranes exhibiting exceptionally high propylene/propane separation. *J. Am. Chem. Soc.* **2013**, *135*, 10763–10768. [[CrossRef](#)] [[PubMed](#)]
33. Huang, A.; Dou, W.; Caro, J. Steam-stable zeolitic imidazolate framework ZIF-90 membrane with hydrogen selectivity through covalent functionalization. *J. Am. Chem. Soc.* **2010**, *132*, 15562–15564. [[CrossRef](#)] [[PubMed](#)]
34. Caro, J.; Noack, M. Zeolite membranes—recent developments and progress. *Microporous Mesoporous Mater.* **2008**, *115*, 215–233. [[CrossRef](#)]
35. Lin, Y.; Kumakiri, I.; Nair, B.; Alsayouri, H. Microporous inorganic membranes. *Sep. Purif. Methods* **2002**, *31*, 229–379. [[CrossRef](#)]
36. Snyder, M.A.; Tsapatsis, M. Hierarchical nanomanufacturing: From shaped zeolite nanoparticles to high-performance separation membranes. *Angew. Chem. Int. Ed.* **2007**, *46*, 7560–7573. [[CrossRef](#)]
37. Bayati, B.; Ghorbani, A.; Ghasemzadeh, K.; Iulianelli, A.; Basile, A. Study on the separation of H₂ from CO₂ using a ZIF-8 membrane by molecular simulation and maxwell-stefan model. *Molecules* **2019**, *24*, 4350. [[CrossRef](#)]
38. Sun, C.-Y.; Qin, C.; Wang, X.-L.; Yang, G.-S.; Shao, K.-Z.; Lan, Y.-Q.; Su, Z.-M.; Huang, P.; Wang, C.-G.; Wang, E.-B. Zeolitic imidazolate framework-8 as efficient pH-sensitive drug delivery vehicle. *Dalton Trans.* **2012**, *41*, 6906–6909. [[CrossRef](#)]
39. Qin, J.-S.; Du, D.-Y.; Li, W.-L.; Zhang, J.-P.; Li, S.-L.; Su, Z.-M.; Wang, X.-L.; Xu, Q.; Shao, K.-Z.; Lan, Y.-Q. N-rich zeolite-like metal-organic framework with sodalite topology: High CO₂ uptake, selective gas adsorption and efficient drug delivery. *Chem. Sci.* **2012**, *3*, 2114–2118. [[CrossRef](#)]
40. Hao, J.; Stavljenić Milašin, I.; Batu Eken, Z.; Mravak-Stipetic, M.; Pavelić, K.; Ozer, F. Effects of zeolite as a drug delivery system on cancer therapy: A systematic review. *Molecules*. **2021**, *26*, 6196. [[CrossRef](#)]
41. Banerjee, R.; Furukawa, H.; Britt, D.; Knobler, C.; O’Keeffe, M.; Yaghi, O.M. Control of pore size and functionality in isorecticular zeolitic imidazolate frameworks and their carbon dioxide selective capture properties. *J. Am. Chem. Soc.* **2009**, *131*, 3875–3877. [[CrossRef](#)] [[PubMed](#)]
42. Wang, B.; Côté, A.P.; Furukawa, H.; O’Keeffe, M.; Yaghi, O.M. Colossal cages in zeolitic imidazolate frameworks as selective carbon dioxide reservoirs. *Nature* **2008**, *453*, 207–211. [[CrossRef](#)] [[PubMed](#)]
43. Low, J.J.; Benin, A.I.; Jakubczak, P.; Abrahamian, J.F.; Faheem, S.A.; Willis, R.R. Virtual high throughput screening confirmed experimentally: Porous coordination polymer hydration. *J. Am. Chem. Soc.* **2009**, *131*, 15834–15842. [[CrossRef](#)]
44. Schoencker, P.M.; Carson, C.G.; Jasuja, H.; Flemming, C.J.; Walton, K.S. Effect of water adsorption on retention of structure and surface area of metal-organic frameworks. *Ind. Eng. Chem. Res.* **2012**, *51*, 6513–6519. [[CrossRef](#)]
45. Cychosz, K.A.; Matzger, A.J. Water stability of microporous coordination polymers and the adsorption of pharmaceuticals from water. *Langmuir* **2010**, *26*, 17198–17202. [[CrossRef](#)] [[PubMed](#)]
46. Bezverkhyy, I.; Ortiz, G.; Chaplais, G.; Marichal, C.; Weber, G.; Bellat, J.-P. MIL-53 (Al) under reflux in water: Formation of γ -AlO(OH) shell and H₂BDC molecules intercalated into the pores. *Microporous Mesoporous Mater.* **2014**, *183*, 156–161. [[CrossRef](#)]
47. Aguado, S.; Canivet, J.; Schuurman, Y.; Farrusseng, D. Tuning the activity by controlling the wettability of MOF eggshell catalysts: A quantitative structure-activity study. *J. Catal.* **2011**, *284*, 207–214. [[CrossRef](#)]
48. Park, K.S.; Ni, Z.; Côté, A.P.; Choi, J.Y.; Huang, R.; Uribe-Romo, F.J.; Chae, H.K.; O’Keeffe, M.; Yaghi, O.M. Exceptional chemical and thermal stability of zeolitic imidazolate frameworks. *Proc. Natl. Acad. Sci. USA* **2006**, *103*, 10186–10191. [[CrossRef](#)]
49. Morris, W.; He, N.; Ray, K.G.; Klonowski, P.; Furukawa, H.; Daniels, I.N.; Houndonougbo, Y.A.; Asta, M.; Yaghi, O.M.; Laird, B.B. A combined experimental-computational study on the effect of topology on carbon dioxide adsorption in zeolitic imidazolate frameworks. *J. Phys. Chem. C* **2012**, *116*, 24084–24090. [[CrossRef](#)]

50. Zeeshan, M.; Keskin, S.; Uzun, A. Enhancing CO₂/CH₄ and CO₂/N₂ separation performances of ZIF-8 by post-synthesis modification with [BMIM][SCN]. *Polyhedron* **2018**, *155*, 485–492. [[CrossRef](#)]
51. Aguado, S.; Canivet, J.; Farrusseng, D. Facile shaping of an imidazolate-based MOF on ceramic beads for adsorption and catalytic applications. *Chem. Commun.* **2010**, *46*, 7999–8001. [[CrossRef](#)] [[PubMed](#)]
52. Tsuruoka, T.; Furukawa, S.; Takashima, Y.; Yoshida, K.; Isoda, S.; Kitagawa, S. Nanoporous Nanorods Fabricated by Coordination Modulation and Oriented Attachment Growth. *Angew. Chem. Int. Ed.* **2009**, *48*, 4739–4743. [[CrossRef](#)] [[PubMed](#)]
53. Baias, M.; Lesage, A.; Aguado, S.; Canivet, J.; Moizan-Basle, V.; Audebrand, N.; Farrusseng, D.; Emsley, L. Superstructure of a Substituted Zeolitic Imidazolate Metal–Organic Framework Determined by Combining Proton Solid-State NMR Spectroscopy and DFT Calculations. *Angew. Chem. Int. Ed.* **2015**, *54*, 5971–5976. [[CrossRef](#)] [[PubMed](#)]
54. Shi, Q.; Wang, J.; Shang, H.; Bai, H.; Zhao, Y.; Yang, J.; Dong, J.; Li, J. Effective CH₄ enrichment from N₂ by SIM-1 via a strong adsorption potential SOD cage. *Sep. Purif. Technol.* **2020**, *230*, 115850. [[CrossRef](#)]
55. Johnson, T.; Lozińska, M.M.; Orsi, A.F.; Wright, P.A.; Hindocha, S.; Poulston, S. Improvements to the production of ZIF-94; a case study in MOF scale-up. *Green Chem.* **2019**, *21*, 5665–5670. [[CrossRef](#)]
56. Al-Naddaf, Q.; Lawson, S.; Rownaghi, A.A.; Rezaei, F. Analysis of dynamic CO₂ capture over 13X zeolite monoliths in the presence of SO_x, NO_x and humidity. *AIChE J.* **2020**, *66*, e16297. [[CrossRef](#)]
57. Yang, L.-Y.; Cao, J.-H.; Cai, B.-R.; Liang, T.; Wu, D.-Y. Electrospun MOF/PAN composite separator with superior electrochemical performances for high energy density lithium batteries. *Electrochim. Acta* **2021**, *382*, 138346. [[CrossRef](#)]
58. Aguado, S.; Quirós, J.; Canivet, J.; Farrusseng, D.; Boltes, K.; Rosal, R. Antimicrobial activity of cobalt imidazolate metal–organic frameworks. *Chemosphere* **2014**, *113*, 188–192. [[CrossRef](#)]
59. Mendiola-Alvarez, S.Y.; Palomino, G.T.; Guzmán-Mar, J.; Hernández-Ramírez, A.; Hinojosa-Reyes, L.; Cabello, C.P. Magnetic porous carbons derived from cobalt (ii)-based metal–organic frameworks for the solid-phase extraction of sulfonamides. *Dalton Trans.* **2020**, *49*, 8959–8966. [[CrossRef](#)]
60. Quirós, J.; Boltes, K.; Aguado, S.; de Villoria, R.G.; Vilatela, J.J.; Rosal, R. Antimicrobial metal–organic frameworks incorporated into electrospun fibers. *Chem. Eng. J.* **2015**, *262*, 189–197. [[CrossRef](#)]
61. Myers, P. Thermodynamics of mixed gas adsorption. *AIChE J.* **1965**, *11*, 121–131. [[CrossRef](#)]
62. Liu, B.; Smit, B. Molecular simulation studies of separation of CO₂/N₂, CO₂/CH₄, and CH₄/N₂ by ZIFs. *J. Phys. Chem. C* **2010**, *114*, 8515–8522. [[CrossRef](#)]
63. Battisti, A.; Taioli, S.; Garberoglio, G. Zeolitic imidazolate frameworks for separation of binary mixtures of CO₂, CH₄, N₂ and H₂: A computer simulation investigation. *Microporous Mesoporous Mater.* **2011**, *143*, 46–53. [[CrossRef](#)]
64. Thomas, A.; Prakash, M. Ionic liquid incorporation in zeolitic imidazolate framework-3 for improved CO₂ separation: A computational approach. *Appl. Surf. Sci.* **2021**, *562*, 150173. [[CrossRef](#)]
65. Wang, Y.; Jin, H.; Ma, Q.; Mo, K.; Mao, H.; Feldhoff, A.; Cao, X.; Li, Y.; Pan, F.; Jiang, Z. A MOF Glass Membrane for Gas Separation. *Angew. Chem. Int. Ed.* **2020**, *59*, 4365–4369. [[CrossRef](#)]
66. Han, J.; Bai, L.; Jiang, H.; Zeng, S.; Yang, B.; Bai, Y.; Zhang, X. Task-specific ionic liquids tuning ZIF-67/PIM-1 mixed matrix membranes for efficient CO₂ separation. *Ind. Eng. Chem. Res.* **2020**, *60*, 593–603. [[CrossRef](#)]
67. Wu, Y.; Lv, Z.; Zhou, X.; Peng, J.; Tang, Y.; Li, Z. Tuning secondary building unit of Cu-BTC to simultaneously enhance its CO₂ selective adsorption and stability under moisture. *Chem. Eng. J.* **2019**, *355*, 815–821. [[CrossRef](#)]
68. Kulak, H.; Polat, H.M.; Kavak, S.; Keskin, S.; Uzun, A. Improving CO₂ Separation Performance of MIL-53 (Al) by Incorporating 1-n-Butyl-3-Methylimidazolium Methyl Sulfate. *Energy Technol.* **2019**, *7*, 1900157. [[CrossRef](#)]
69. Zhou, Z.; Mei, L.; Ma, C.; Xu, F.; Xiao, J.; Xia, Q.; Li, Z. A novel bimetallic MIL-101 (Cr, Mg) with high CO₂ adsorption capacity and CO₂/N₂ selectivity. *Chem. Eng. Sci.* **2016**, *147*, 109–117. [[CrossRef](#)]
70. Hu, Z.; Zhang, K.; Zhang, M.; Guo, Z.; Jiang, J.; Zhao, D. A Combinatorial Approach towards Water-Stable Metal–Organic Frameworks for Highly Efficient Carbon Dioxide Separation. *ChemSusChem* **2014**, *7*, 2791–2795. [[CrossRef](#)]
71. Lou, W.; Yang, J.; Li, L.; Li, J. Adsorption and separation of CO₂ on Fe (II)-MOF-74: Effect of the open metal coordination site. *J. Solid State Chem.* **2014**, *213*, 224–228. [[CrossRef](#)]
72. Chen, C.; Feng, X.; Zhu, Q.; Dong, R.; Yang, R.; Cheng, Y.; He, C. Microwave-assisted rapid synthesis of well-shaped MOF-74 (Ni) for CO₂ efficient capture. *Inorg. Chem.* **2019**, *58*, 2717–2728. [[CrossRef](#)] [[PubMed](#)]
73. Bae, T.H.; Long, J.R. CO₂/N₂ Separations with Mixed-Matrix Membranes Containing Mg₂(dobdc) Nanocrystals. *Energy Environ. Sci.* **2013**, *6*, 3565–3569. [[CrossRef](#)]
74. Masala, A.; Vitillo, J.G.; Bonino, F.; Manzoli, M.; Grande, C.A.; Bordiga, S. New insights into UTSA-16. *Phys. Chem. Chem. Phys.* **2016**, *18*, 220–227. [[CrossRef](#)] [[PubMed](#)]
75. Lin, J.B.; Nguyen, T.T.; Vaidhyanathan, R.; Burner, J.; Taylor, J.M.; Durekova, H.; Shimizu, G.K. A scalable metal-organic framework as a durable physisorbent for carbon dioxide capture. *Science* **2021**, *374*, 1464–1469. [[CrossRef](#)]
76. Chen, C.; Yu, Y.; He, C.; Wang, L.; Huang, H.; Albilali, R.; Hao, Z. Efficient capture of CO₂ over ordered micro-mesoporous hybrid carbon nanosphere. *Appl. Surf. Sci.* **2018**, *439*, 113–121. [[CrossRef](#)]
77. Chen, C.; Huang, H.; Yu, Y.; Shi, J.; He, C.; Albilali, R.; Pan, H. Template-free synthesis of hierarchical porous carbon with controlled morphology for CO₂ efficient capture. *Chem. Eng. J.* **2018**, *353*, 584–594. [[CrossRef](#)]
78. Kou, J.; Sun, L.B. Fabrication of nitrogen-doped porous carbons for highly efficient CO₂ capture: Rational choice of a polymer precursor. *J. Mater. Chem. A* **2016**, *4*, 17299–17307. [[CrossRef](#)]

79. McEwen, J.; Hayman, J.D.; Yazaydin, A.O. A comparative study of CO₂, CH₄ and N₂ adsorption in ZIF-8, Zeolite-13X and BPL activated carbon. *Chem. Phys.* **2013**, *412*, 72–76. [[CrossRef](#)]
80. Wang, C.; Liu, J.; Yang, J.; Li, J. A crystal seeds-assisted synthesis of microporous and mesoporous silicalite-1 and their CO₂/N₂/CH₄/C₂H₆ adsorption properties. *Microporous Mesoporous Mater.* **2017**, *242*, 231–237. [[CrossRef](#)]